SMALL SCALE PRODUCTION IN THE COHERENT STRUCTURES OF A SHEAR FLOW OVER AN OPEN CAVITY

Laurent Jacquin
Department of Fundamental and Experimental Aerodynamics
ONERA, 8, rue des Vertugadins, 92190 Meudon– France
Jacquin@onera.fr

Nicolas Forestier
Same address, forest@onera.fr

Philippe Geffroy
Same address, geffroy@onera.fr

ABSTRACT

The present study aims at showing an example of shear flow in which small scale perturbations are directly produced inside strongly organized vortex or coherent structures. The flow under consideration is a mixing layer which develops over a cavity in a high speed flow where it is forced by a low frequency acoustic resonance. The mixing layer is observed to organize itself into highly coherent 2D vortices which have been scrutinized by means of a conditional LDV technique as in Lyn & Rodi (1995). When considering the triple decomposition of the flow velocity which discriminates the "coherent" motion (phase average) from the random motion, it is observed that the latter concentrates into the vortex cores. A detailed analysis of the flow indicates that a linear elliptic instability mechanism could be responsible of this small scale production. This departs from the classical picture where small scale turbulence is preferentially produced by continual stretching of three-dimensional vorticity in the saddle regions between vortical structures. This difference could be attributed to the highly coherent organization of the vorticity which is found in a cavity flow and which is rarely encountered in other forced mixing layers.

INTRODUCTION

In canonical mixing layers, once coherent structures are formed through successive pairing of Kelvin-Helmhotz vortices, one usually observes that small scale fluctuations are produced through continual stretching of three-dimensional vorticity in the saddle regions between the vortical structures, see Cantwell & Coles (1983) and Hussain & Hayakawa (1987). This is recognised as the main mechanism responsible for small scale turbulent production in equilibrium or forced mixing layers. In particular, high levels of phase-averaged small scale production by the Reynolds shear stress are identified in the saddle regions.

In the flow which develops over an open cavity the mixing layer acquires a much coherent dynamics due to a strong resonant forcing. In a transonic regime, forcing is due to discrete tones which are characteristic of a feedback mechanism between the mixing layer development and the pressure fluctuations generated at the downstream edge of the cavity, see Rossiter (1966), Rockwell & Naudascher (1979). Strong variations of pressure, density and side forces result from this flow/acoustic resonance. One of the first database devoted to the flow-field description of such flows has been recently provided by Forestier et al. (2001). Visualisations show that coherent structures are formed after a rapid roll-up of the separated boundary layer in phase with pressure oscillations. These highly coherent eddies form at frequencies lower than the natural shear layer frequency so that the flow amounts to a shear layer under a strong low frequency forcing. Same phenomenon is also observed in similar flows as impinging jet, jet screech and edge tones. In the case of high speed jets impinging on a flat plate, Ho & Nosseir (1981) attributed this formation process of large scale structures to a 'collective interaction mechanism' described by Ho & Huang (1982). In this regime, one observes that the strong low frequency forcing leads to "by-passing" of the pairing and vorticity stretching mechanisms which drive the growth of natural or weakly forced mixing layers (Winant & Browand, 1974). The Kelvin-Helmholtz eddies merge rapidly due to the forcing and result in the formation of large scale structures within small distances. As shown by Forestier et al. (2001), 'collective interaction' seems also to hold in the cavity flows, as already suggested by Gharib & Roshko (1987).

Small scale perturbations which are superimposed on the train of periodic eddies represent nearly half the total kinetic energy of the fluctuations (Forestier et al., 2001). These small scale structures are convected from the separated boundary layer (which is turbulent) and are also produced by the shear. Using standard conditional procedures to separate the velocity field into phase averaged and random parts, one finds that small scale production regions

coincide with coherent structure centres, a result which departs from what is usually observed in canonical flows.

Cavity flows constitute a generic problem for aero-acoustics, aero-optics and aero-elasticity applications. Understanding how the small scales develop within such a flow and how they may extract energy to coherent eddies is an important issue for the control of such flows.

EXPERIMENTAL SET-UP

The flow is produced by a boundary layer separating on a deep cavity of aspect L/D=0.42 where $L = 50mm$ is the length of the cavity, $D = 120mm$ its depth and $S = 120mm$, its span, see figure 1. This experimental set-up is placed in a continuous transonic wind tunnel whose test section is 100x120 mm^2. The free stream Mach number and velocity are $M_e = 0.8$, $U_e = 258ms^{-1}$. The measurements comprise schlieren visualizations and conditional analysis of LDV signals controlled by a pressure signal delivered by a *Kulite*™ sensor located in the upstream vertical wall of the cavity (a series of 5 sensors is visible in figure 1). Details are given in Forestier et al, (1999, 2001). The complete data comprises conditional LDV measurements performed in several regions. The results shown below corresponds to the symmetry vertical plane $y = 0$ and to the horizontal plane $z = 0$, which are surveyed with a constant mesh size $\Delta x = \Delta z = 2\ mm$ and $\Delta x = \Delta y = 5\ mm$, respectively.

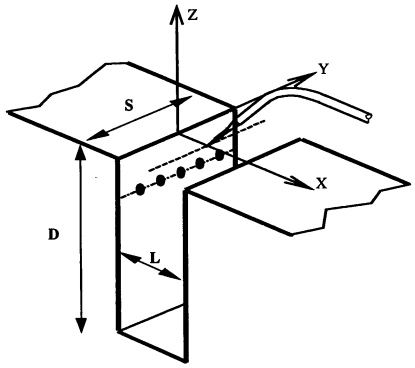

Figure 1: Cavity model

CHARACTERISTIC REGIONS OF THE FLOW

The shear layer expansion is characterised in figure 2 through the variation of the incompressible momentum thickness θ :

$$\theta = \int_{z_{min}}^{z_{max}} \frac{\overline{U}}{U_e}\left(1-\frac{\overline{U}}{U_e}\right) dz \qquad (1)$$

where $z_{min} = -12mm$ and $z_{max} = 12mm$ correspond to the vertical location of the lower and upper mesh boundaries. Normalisation is made with the initial value $\theta_0 = 0.648\ mm$ measured $1mm$ ahead of the upstream cavity edge. The momentum thickness θ calculated with (1) may differ from the standard definition used for free shear layers, e.g. $z_{min} \to -\infty$, $z_{max} \to \infty$, if $\overline{U}(x, z_{min})$ and/or $\overline{U}(x, z_{max})$ have not reached a constant value. However, deviations are expected to be small except near the downstream end of the domain where interaction with the wall occurs.

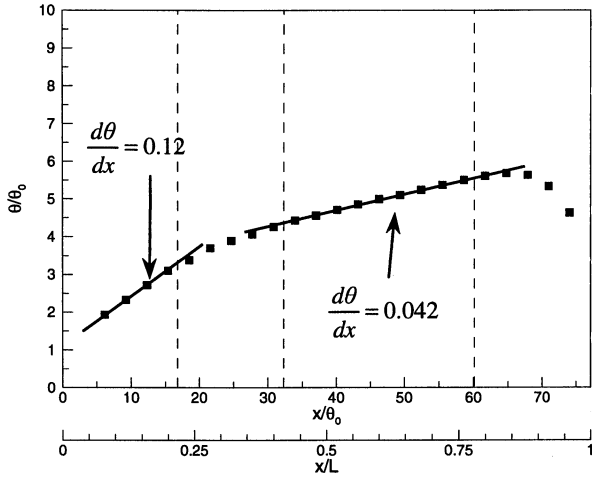

Figure 2 : Momentum thickness of the mixing layer. θ_0 is the initial momentum thickness at $x = -1\ mm$.

From figure 2, three regions may be defined. In region 1, $0 \le x/\theta_0 \le 17$, the momentum thickness grows linearly with a growth rate equal to 0.12. This value is nearly three times larger than that found in equilibrium free shear layers. A possible interpretation of this high initial spreading rate is the 'collective interaction mechanism' evoked in the introduction. In region 2, $32 \le x/\theta_0 \le 60$, the growth rate has decreased to 0.042, a value close to that found in free turbulent mixing layers. As an example, Browand and Trout (1985) found $d\theta/dx = 0.034\,\lambda$ with $\lambda = \Delta U/2\overline{U}$ and $\overline{U}$ the mean velocity of the two flows and ΔU, the velocity difference. Neglecting the mean flow recirculation in the cavity leads to $\lambda \approx 1$. Ho (1986) observed that, after a 'collective interaction', the flow of Ho & Huang (1982) resumes a classical growth rate beyond $\lambda x/\theta_0 \approx 20$, a value which may be compared to $\lambda x/\theta_0 \approx 32$ found here with $\lambda \approx 1$. Detailed analysis shows that the flow is not self preserving within region 2 (see Forestier et al., 2001). In region 3, $60 \le x/\theta_0 \le 77$, the momentum thickness decreases as the flow approaches the downstream edge of the cavity. The extent of region 3, which is 17 initial momentum thickness, characterises the influence of the downstream corner. The final decrease of the momentum thickness in figure 2 results from the break-up of the flow but also from a

lack of spatial resolution when using (1). Region 3 is characterised by a violent inflow/outflow motion.

CONDITIONAL ANALYSIS

As shown in figure 3, the flow is forced by a highly periodic pressure fluctuation (of about $155dB$), dominated by the first cavity frequency mode.

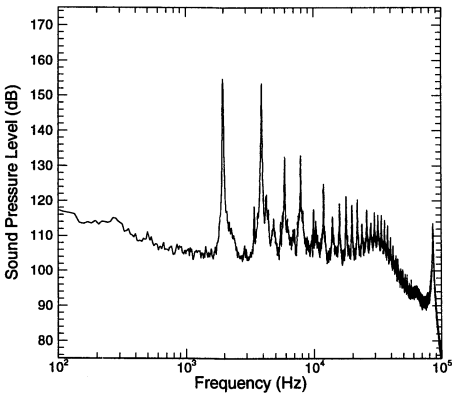

Figure 3 : Spectrum of the pressure signal delivered by a *Kulite*™ sensor located on the upstream vertical wall at $x=0, y=0, z=-35\ mm$.

This leads to the rapid organization of the flow into three individual vortex structures which travel through the flow following different trajectories, as shown in figure 4 where a schlieren picture and a sample result of the phase averaging are compared.

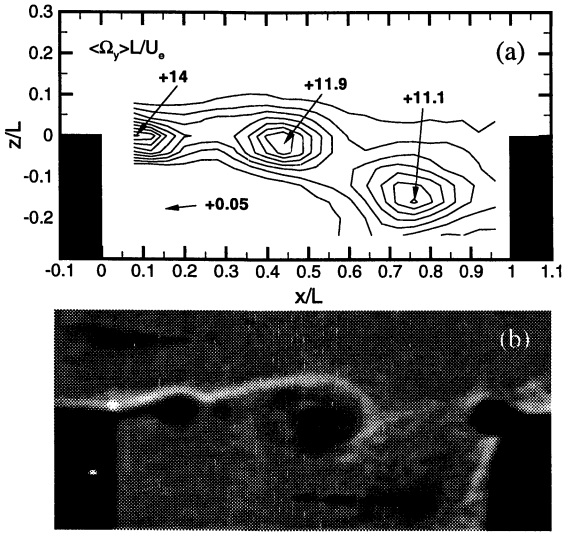

Figure 4 : (a) Contour plots of the phase averaged spanwise vorticity $<\Omega_y>L/U_e$ (phase 20), (b) Schlieren image

The standard triple decomposition $\underline{u}(\underline{x},t)=\overline{\underline{u}}(\underline{x})+\tilde{\underline{u}}(\underline{x},t)+\underline{u}'(\underline{x},t)$ is used where $\overline{\underline{u}}(\underline{x})$ denotes a temporal average, $\tilde{\underline{u}}(\underline{x},t)$, the coherent part of the fluctuation and $\underline{u}'(\underline{x},t)$, the random part. The phase average is $<\underline{u}>(\underline{x},t)=\overline{\underline{u}}(\underline{x})+\tilde{\underline{u}}(\underline{x},t)$. The films and the velocity field analysis shows that the three structures do not merge. Figure 5 shows the case of phase 17 where two of the structures seen in figure 4 are moving at the same convection velocity. The pseudo-streamlines in a frame moving at this convection velocity are sketched in figure 5(a). These streamlines have been obtained using the *Tecplot*™ streamline routine without any further post-processing. We have indicated the points C_1 and C_2 which correspond to the position of the centres of the structures and the point S which corresponds to the saddle point. The spiral shape of the first structure (characterized by the centre C_1) may denote three-dimensional effects. The strong 2D organization of the flow is illustrated in figure 5(b) and (c) which show the vorticity distribution in the vertical plane $y=0$ and results of measurements performed in the horizontal plane $z=0$. Figures 5(d) and (e) show that the maximum of random fluctuation kinetic energy, $<u'^2>/U_e^2$, $<w'^2>/U_e^2$

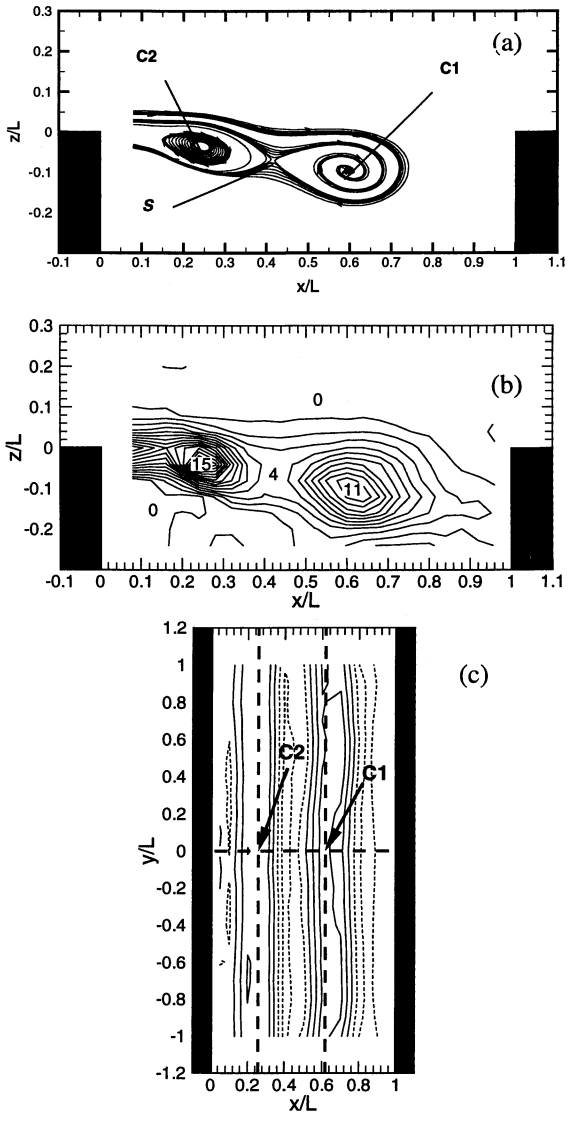

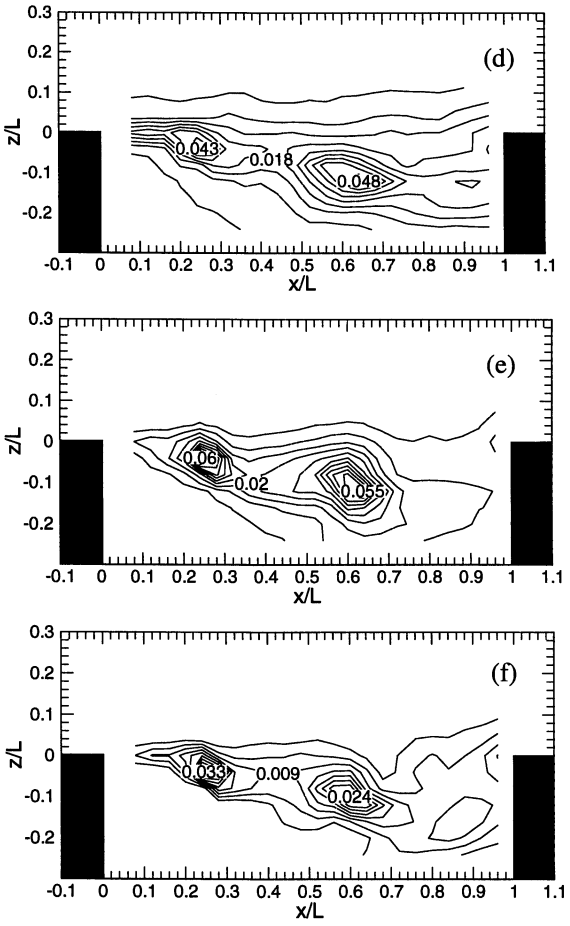

Figure 5 : Contour plots for phase 17 (among 20) of various phase averages : (a) pseudo-streamlines in a frame convected at the convection velocity of the two structures, iso-levels of : (b) vorticity $<\Omega_y> L/U_e$, (c) $-\partial <W>/\partial x$ in the plane z=0, (d) $<u'^2>/U_e^2$ (level increment step of 0.005), (e) $<w'^2>/U_e^2$ (same increment step), (f) $<-u'w'>/U_e^2$ (level increment step of 0.003).

are located within the vortex cores. This is a common trend to all mixing layer experiments where such quantities have been characterized. However, maximum of $-<u'w'>$ is usually found in the saddle regions and not in the structure centers as observed in figure 5(f).

Production of random perturbation kinetic energy from the phase averaged mean flow is due to the following terms $<P>=<P_n>+<P_s>$ where :

$$\begin{cases} <P_n> = -<u'^2>\dfrac{\partial <U>}{\partial x} - <w'^2>\dfrac{\partial <W>}{\partial z} \\ <P_s> = -<u'w'>\left(\dfrac{\partial <U>}{\partial z} + \dfrac{\partial <W>}{\partial x}\right) \end{cases} \qquad (2)$$

$<P> L/U_e^3$ is shown in figure 6(a) and is found to be essentially positive with maximum in the vortex cores. Most of the contribution to $<P>$ comes from $<P_s>$.

DISCUSSION

It has been checked that measurement bias, such as the effect of vortex meandering from period to period, see Hussain (1986), or seeding particle

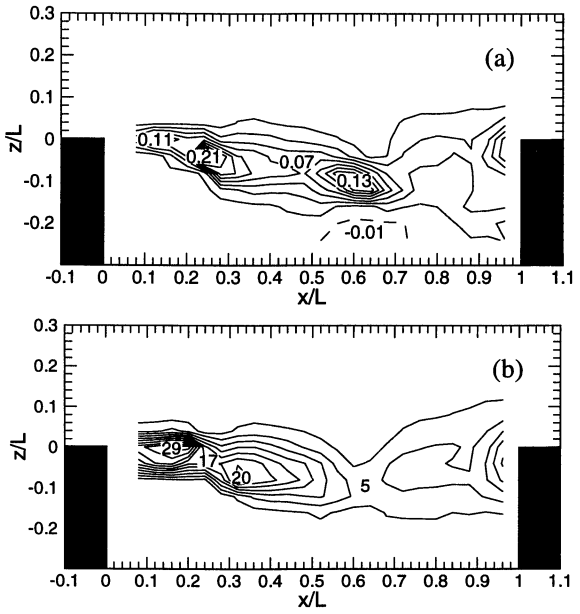

Figure 6 : Contour plots for phase 17 (among 20) of various phase averages : (a) production of random fluctuations $<P> L/U_e^3$ (b) strain rate $<S>^2 L^2/U_e^2$, where $<S>^2 = <\underline{\underline{d}}> : {}^t<\underline{\underline{d}}>$, $\underline{\underline{d}} = \left(\underline{\underline{\nabla u}} + {}^t\underline{\underline{\nabla u}}\right)/2$.

centrifugation, are not responsible for the peculiar distribution of the shear stress distribution found here, see Forestier et al. (2001).

Strong small scale fluctuations within the spanwise vortex cores have been observed in direct numerical simulations, especially when pairing is suppressed (see e.g. Metcalfe et al., 1987). A possible physical mechanism which could promote the production of these fluctuations is the elliptic instability which occurs in elliptically shaped streamlines of two-dimensional flows (see Pierrehumbert, 1986, Bayly, 1988, Moore & Saffman, 1975, Waleffe, 1990). The role of these instabilities in coherent structures has been first studied by Pierrehumbert & Widnall (1982). They have identified the existence of a broadband spectrum of three-dimensional instabilities, most visible in the central region of the vortices, which is able to produce small-scale turbulence. A general theory of these elliptic instabilities has been established later (see references above). Elliptic instabilities result from the stretching of vorticity perturbations by a strain field whose rate is proportional to the ellipticity of the streamline. Figure 7 shows that this instability does produce a distribution of shear stress which is concentrated in the central region of the vortex. This figure shows results of the linearised Euler equations in the asymptotic limit of a weak strain rate (i.e. for a small

deformation of the streamlines, see Moore & Saffman, 1975). The background flow is a Lamb-Oseen vortex corresponding to phase-averaged spanwise vorticity field :

$$<\Omega_y>(x,z)=\exp\left\{-\left(x^2+z^2\right)\right\}, \qquad (3)$$

with a unit characteristic radius and a $\Gamma=2\pi$ circulation. One superposes on this flow a strain field of rate $\varepsilon<<1$ with an extension axis oriented at 45° with respect to the vertical. The resulting velocity gradient reads :

$$\underline{\underline{\nabla u}}=\begin{pmatrix}0 & \varepsilon+\gamma\\ \varepsilon-\gamma & 0\end{pmatrix} \qquad (4)$$

where $\gamma(x,z)$ denotes the rotation rate of the vortex, an evaluation of which is $\gamma(x,z)=<\Omega_y>(x,z)/2$. Figure 7(a) shows the spanwise vorticity perturbation field ω_y' of the most amplified mode of the elliptical instability. This perturbation grows with the characteristic time scale $\tau_{elliptic}=C/\varepsilon$, where C is a constant close to 0.5 (in the asymptotic limit $\varepsilon/\gamma\to 0$, $C=9/16$) and exhibits a dipolar structure which is characteristic of this instability (see Waleffe, 1990 and figure 8 of Pierrehumbert & Widnall, 1982). Iso-values of $-u'w'$ are plotted in figure 7(b). They look like those obtained in the experiment: the product $-u'w'$ is positive and the maximum is located in the vortex centre. This shows that the elliptic instability could contribute to a distribution of the shear stress localised in the vortex centre, as in the present experiment. However, a more quantitative check is necessary to comfort this conjecture. In particular, one must evaluate if the instability has time to develop within the convection time scale of the structures. Given a vortex structure labelled S, $\tau_c^S(x)\equiv\int_0^x dx/U_c^S(x)$ defines the time the structure takes to reach the downstream position x with a convection velocity $U_c^S(x)$. These time scales have been deduced from inspection of the centroïd paths which are reported in figure 8. Considering the characteristic distances x_1 and x_2 which correspond to the downstream limit of region 1 and to the upstream limit of region 2, as defined in figure 2, the times it takes for a structure to cover these distances starting from their origin is found to be $\tau_c^{S1}(x_1)U_e/L\approx 0.5$ and $\tau_c^{S1}(x_2)U_e/L\approx 1$ for structure S_1. Same values are obtained for structure S_2. This leads to the following characteristic time scales : $\tau_c^S(x_1)\approx 100\mu s$, $\tau_c^S(x_2)\approx 200\mu s$. Now, a crude evaluation of the time scale $\tau_{elliptic}=C/\varepsilon$, may be done as follows. Inspection of the shape of the structures depicted in figure 5(a), shows that they

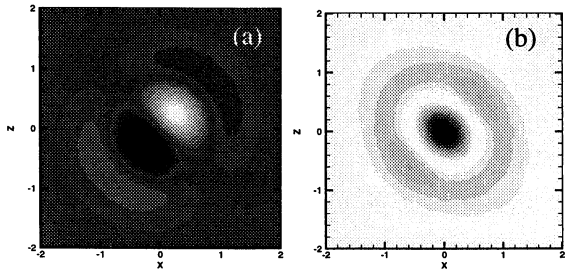

Figure 7 : Elliptic instability in the Lamb-Oseen vortex subjected to a 45° strain : (a) fluctuation of the spanwise vorticity $\omega_y'(x,z,t)$ of the most amplified mode (arbitrary levels), (b) shear stress $-u'w'(x,z,t)$ (arbitrary levels).

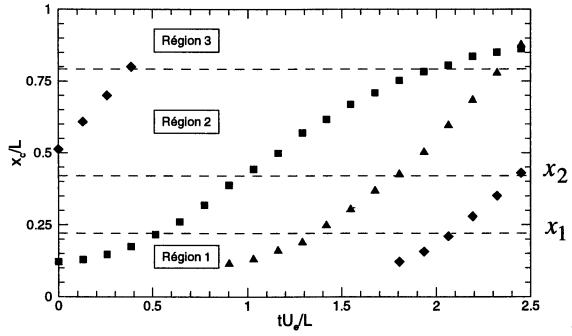

Figure 8. Vorticity centroid position versus time : structure S_1 (square), structure S_2 (triangle), structure S_3 (diamond). The time origin is arbitrary

are elliptical with a typical aspect ratio (ratio between major and minor axis) $E\approx 2$ and a slight incidence. It can be shown that in the central region of such a strained vortex, the aspect ratio of the streamlines is $E\approx\sqrt{(\gamma+\varepsilon)/(\gamma-\varepsilon)}$ where γ is the rotation rate and $\gamma>\varepsilon$. For $E\approx 2$, this gives $\varepsilon/\gamma\approx 3/5$. Using $\gamma\approx<\Omega_y>_{\max}/2$ for the rotation rate, a characteristic value is $<\Omega_y>_{\max}L/U_e\approx 15$ for structure S_2 at the end of region 1, see figure 5(b). This leads to $\varepsilon\approx 3\gamma/5\approx 23\,kHz$. This estimate, based on the global shape of the flow streamlines, is supported by comparisons to the phase-averaged strain rate shown in figure 6(b) : using the above evaluation $\varepsilon\approx 23\,kHz$ leads to $\varepsilon^2L^2/U_e^2\approx 20$, a value close to $<S>^2L^2/U_e^2\approx 17$ found in figure 6(b) in the centre C_2 of structure S_2. Now, correction must be done to account for the effect of the mesh size on which the exact values of $<\Omega_y>$ and $<S>$ may depend. The value $\varepsilon\approx 23\,kHz$ obtained above is a minimum. Tests have shown that $<\Omega_y>_{\max}$ may increase by a factor of 2-3 when the mesh size is decreased by a factor of 8 from $\Delta x=\Delta z=2\,mm$ to $0.25\,mm$. As a conclusion, application of a factor of nearly 2 on $<\Omega_y>$ is a reasonable choice. Applying this factor to ε leads to a new estimation $\varepsilon\approx 45\,kHz$.

After all, an estimation of the time scale of the instability is $\tau_{elliptic} \approx 1/(0.5\,\varepsilon) \approx 45\,\mu s$ to be compared with $\tau_c^S(x_1) \approx 100\,\mu s$ or $\tau_c^S(x_2) \approx 200\,\mu s$ Consequently, when crossing region 1, initial perturbations within the structures are amplified by a factor e^2 at $x = x_1$. This indicates that the flow is still at the beginning of the linear regime in this region. If the flow were initially in a laminar regime, development of very small initial perturbations with such a time scale would not be significant. But the elliptic structures contain energetic perturbations coming from the turbulent boundary layer. The strain field associated to the streamline ellipticity then amounts to a distortion of this turbulence to which it supplies energy and imposes a preferential orientation (see Cambon & Scott, 1999).

CONCLUSION

The mixing layer which develops over an open cavity is subjected to a strong forcing at low frequency which forces the flow into a train of very coherent eddies. The kinetic energy of the random perturbations is concentrated in the central region of the structures, as it is observed in other studies on forced mixing layers. This may result from transport of turbulence produced by stretching in the saddle regions, as advocated by other authors, but also by the local influence of elliptic instabilities. A better conservation of this energy due to decrease of dissipation by rotation, a mechanism which characterises highly swirling flows, can also be advocated. But among all the above mentioned mechanisms, only the elliptic instability mechanism seems compatible with the additional observation of a Gaussian like distribution of the shear stress $-<u'w'>$ within the vortex cores. This would indicate that this mechanism plays an important role in the coupling between large and small scales in this flow where turbulence is not yet fully developed.

Acknowledgements

This research has been conducted in the frame of the ONERA Research Project "Mesure et Modélisation Numérique de la Turbulence". Part of this work has been supported by Service des Programmes Aéronautique. The Laser Doppler Measurement Group of the Fundamental and Experimental Aerodynamic Department of ONERA is acknowledged for its contribution to the experiment.

REFERENCES

Bayly B.J., 1988, "Three-dimensional instability of inviscid two-dimensional flows", Phys. Fluids 31(1), 56-64.

Browand, F. K. & Troutt, T. R., 1985, "The turbulent mixing layer: geometry of large vortices", *J. Fluid Mech.* 158, 489-509.

Cambon, C. & Scott, J.F., 1999, "Linear and non-linear models of anisotropic turbulence", *Ann. Rev. Fluid Mech.* **31**, 1-53.

Cantwell, B. & Coles, D., 1983, "An experimental study of entrainment and transport in the turbulent near wake of a circular cylinder", *J. Fluid Mech.* 136, 321-374.

Forestier, N., Geffroy, P. & Jacquin, L., 1999, "Flow over cavities in transonic regime: a test case for numerical simulations", Proc. First International Symp. on Turbulence Shear Flow Phenomena, Santa Barbara, CA., 933-938.

Forestier N., Jacquin L. & Geffroy P., 2001, "The flow-field over a deep cavity at high-subsonic speed", submitted to the *J. Fluid Mech.*

Gharib, M. & Roshko, A., 1987, "The effect of flow oscillations on cavity drag", *J. Fluid Mech.*, 177, 501-530.

Ho, C.-M., 1986, "Mixing process in free shear layers", *AIAA Paper* 86-0234.

Ho C.M. & Nosseir, N. S., 1981, "Dynamics of an impinging jet. Part1. The feedback phenomenon", *J. Fluid Mech.*, 105, 119-142.

Ho, C.-M. & Huang, L.-S., 1982, "Subharmonics and vortex merging in mixing layers", *J. Fluid Mech*, 119, 443-473.

Hussain, A. K. M. F., 1986, "Coherent structures and turbulence", *J. Fluid Mech.*, 173, 303-356.

Hussain, A. K. M. F. & Hayakawa, M., 1987, "Eduction of large-organized structures in a turbulent plane wake", *J. Fluid Mech.* 180, 193-229.

Lyn, D. A. & Rodi, W., 1994, "The flapping shear layer formed by flow separation from the forward corner of a square cylinder", *J. Fluid Mech.*, 267, 353-376.

Metcalfe R.W., Orzag S.A., Brachet M., Menon S. & Riley J.J., 1987, "Secondary instability of a temporally growing mixing layer", *J. Fluid Mech.* 184, 207-243.

Moore D.W. & Saffman P.G., 1975, "The instability of a straight vortex filament in a strain field", Proc. Soc. Lond., A, 346, 413-25.

Pierrehumbert, R.T., 1986, "Universal short-wave instability of two dimensional eddies in an inviscid fluid", *Phys. Rev. Lett.* 57 (17), 2157-9.

Pierrehumbert, R. T. & Widnall, S. E., 1982, "The two- and three-dimensional instabilities of a spatially periodic shear layer", *J. Fluid Mech.*, 114, 59-82.

Rockwell, D. & Naudascher, E., 1979, "Self-sustained oscillations of impinging free shear layers", *Ann. Rev. Fluid Mech.*, 11, 67-94.

Rossiter, J. E., 1966, "Wind-tunnel experiments on the flow over rectangular cavities at subsonic and transonic speeds", ARC R&M 3438.

Waleffe F., 1990, "On the three-dimensional instability of strained vortices", *Physics of Fluids* A, (1), 76-80.

Winant, C. D. & Browand, F. K., 1974, "Vortex pairing, the mechanism of turbulent mixing layer growth at moderate Reynolds number", *J. Fluid Mech*, 63, 237-255.